Reaction Paths for the Conversion of Methane to Methanol Catalyzed by FeO^+

Kazunari Yoshizawa,* Yoshihito Shiota, and Tokio Yamabe*

Abstract: We propose possible theoretical reaction paths for the conversion of methane to methanol catalyzed by FeO^+. The geometric and electronic structures for the reactant, product, intermediates, and transition states were calculated and analyzed in detail by means of a hybrid Hartree–Fock/density functional method. Sextet and quartet spin states were taken into consideration in the analysis of the reaction paths. The conversion of methane to methanol was shown to proceed through basic concerted hydrogen- and methyl-shift reactions. A fragment molecular orbital analysis for the formation of the reactant complex, OFe^+-CH_4, which plays an important role in the initial stage of methane activation, was carried out in order to understand the nature of the interesting Fe–C bond. The five-coordinate methane in the reactant complex was calculated to have a C_{3v}-type geometry. Each reaction path presented in this paper includes an important insertion species, $HO-Fe^+-CH_3$ or $H-Fe^+-OCH_3$, and two transition states. Thus, there are several kinds of reaction paths, if the high-spin sextet and low-spin quartet states are taken into consideration. A reaction towards the hydroxy intermediate, $HO-Fe^+-CH_3$, was found to be more favorable in both the sextet and quartet spin states from the viewpoint of activation energy, and this intermediate is extremely stable. It was found from intrinsic reaction coordinate (IRC) analyses that two basic reactions coexist, namely, hydrogen or methyl migration between the reactant and the methoxy intermediate, $H-Fe^+-OCH_3$. This transition state is interesting, because the two transition states resulting from C–H bond cleavage and methyl migration are located in the same region of space on the potential energy surfaces. IRCs are partially shown for the complicated first halves of the total reaction paths.

Keywords
ab initio calculations · methane · methanol · reaction mechanisms · transition metals

Introduction

The activation of methane[1–8] has attracted increased attention in recent years. In particular, the conversion of methane to methanol is of great interest because of the possible role of methanol as fuel in the future. The lack of reactivity of methane is often attributed to the high C–H bond energy of 104 kcal mol^{-1}, its low acidity and basicity, and its lack of a dipole moment. A commercial process for the production of methanol from natural gas, which mainly consists of methane, involves two-step reactions associated with the formation of carbon monoxide, as given in Equation (1).[6] The synthesized

$$CH_4 + H_2O \longrightarrow CO + 3H_2 \quad (2)$$

gas, carbon monoxide, is then converted into methanol by a catalytic process [Eq. (2)].

$$CO + 2H_2 \longrightarrow CH_3OH \quad (2)$$

The conversion of hydrocarbons to the corresponding alcohols is also known to occur in biological systems. The very well-known cytochrome P-450 enzyme,[9–14] which can oxidize a variety of hydrocarbons, has an important iron–porphyrin core structure at the catalytically active center. The enzymatic mechanisms for the selective hydroxylation have been extensively studied. Moreover, methane monooxygenase (MMO),[9–14] a well-known metalloenzyme, catalyzes the hydroxylation of methane as well as other hydrocarbons. Recent X-ray structural studies[15] have shown that the catalytically active site of MMO contains dinuclear non-heme iron centers. The catalytic cycle of these metalloenzymes proceeds, without doubt, through reaction processes which differ from the industrial ones mentioned above, because carbon monoxide is supposed to deactivate the catalytic iron centers of metalloenzymes. We are interested in the conversion of methane to methanol catalyzed by MMO from a theoretical viewpoint.[16, 17] The reaction mechanism for the methane–methanol conversion is still not known for any catalytic system, and its analysis would be helpful for the progress of methane chemistry.

The gas-phase reactions of the C–H and C–C bond activation of small hydrocarbons have been extensively studied in the laboratories of Schwarz[18] and of Armentrout.[19] Schwarz and collaborators[18] have extensively investigated the C–H and

[*] Dr. K. Yoshizawa, Y. Shiota, Prof. Dr. T. Yamabe[+]
Department of Molecular Engineering, Kyoto University
Sakyo-ku, Kyoto 606-01 (Japan)
Fax: Int. code +(75)751-7279
e-mail: kazunari@scl.kyoto-u.ac.jp
[+] Also of the Institute for Fundamental Chemistry
34–4 Takano-Nishihiraki-cho, Sakyo-ku, Kyoto 606 (Japan)

0947-6539/97/0307-1160 $ 17.50+.50/0

C–C bond activation by transition-metal oxide and bare metal cations in the gas phase, both experimentally and theoretically. Detailed analyses of various gas-phase reactions of methane, higher alkanes, alkenes, benzene, and other [C, H, O] compounds with FeO^+ have been carried out by the same group. Among these important gas-phase reactions, the conversion of methane to methanol is of great interest, because of the catalytic and enzymatic functions mentioned above. According to refs. [18a–c], a supposed intermediate, H_3C-Fe^+-OH, created by the gas-phase reaction between methane and FeO^+, decomposes into $FeOH^+ + CH_3^{\bullet}$ (57%), $Fe^+ + CH_3OH$ (41%), and $FeCH_2^+ + H_2O$ (2%). Important geometrical structures as well as relative energies for the hypothesized intermediates of these gas-phase reactions have been calculated at the ECP–DZ (effective core potential–double zeta) level of quantum chemical theory.[18c] These calculations have provided us with very useful information for our investigations.

Armentrout et al.[19] have extensively examined the gas-phase reactions between transition metals and hydrocarbons, hydrogen, water, and so on. In ref. [19h], the mechanism and energetics involved in the gas-phase conversion of methane to methanol, catalyzed by CoO^+, and its reverse reaction was elucidated with guided ion-beam mass spectroscopy. It has been suggested that an insertion intermediate, H_3C-Co^+-OH, plays a role in the conversion of methane to methanol in the gas phase.[19h] An important crossing between high-spin and low-spin potential energy hypersurfaces has been proposed as occurring both in the reactions of $MO^+ + H_2$ and $MO^+ + CH_4$.[18h, 19h] Although early transition-metal oxides such as ScO^+, TiO^+, and VO^+ do not react with methane, it is well-known that oxides of the late transition metals, MnO^+ through NiO^+, do react.[18e, 20]

A lot of theoretical work on methane and C–H activation has been carried out by Saillard and Hoffmann,[21] Goddard et al.,[22] Siegbahn et al.,[23] Ziegler et al.,[24] Morokuma et al.,[25] Sakaki and Ieki,[26] and Cundari.[27] However, to the best of our knowledge, a detailed analysis of the reaction path for the conversion of methane to methanol has not yet been executed. In this paper, we describe systematically the reaction pathways as well as the reactant, product, intermediates, and transition states in the methane–methanol conversion catalyzed by FeO^+ in the gas phase.

Possible reaction paths proposed in this paper proceed through two kinds of important reaction intermediates, $HO-Fe^+-CH_3$ and $H-Fe^+-OCH_3$. We calculated and analyzed in detail the reaction coordinates for the possible multistep reactions for the sextet and quartet spin states. Our theoretical study will be helpful for the understanding of the catalytic and enzymatic functions mentioned above, as well as the gas-phase reaction for methane activation and its conversion to methanol.

Abstract in Japanese:

FeO^+によって触媒されるメタンからメタノールへの転化反応に関する反応経路を理論的に解析した。反応経路に沿って、反応物、生成物、中間体、遷移状態のそれぞれの構造と電子状態をハートリーフォック法と密度汎関数法からなるハイブリッド法を用いて計算し、詳細に解析を行った。反応経路の解析をスピン6重項と4重項について行った結果、メタンからメタノールへの転化反応は協奏的な水素の転位とメチル基の転位によって進行することが分かった。反応の初期に形成される錯体、OFe^+-CH_4、がメタンの活性化に重要な役割を果たし、鉄原子に結合した5配位のメタンは、C_{3v}構造を有することを明らかにした。反応経路には、中間体、$HO-Fe^+-CH_3$、を経由するものと別の中間体、$H-Fe^+-OCH_3$、を経由するものとの2種類が存在し、前者の方がエネルギー的に有利であることが分かった。極限的反応座標(IRC)の解析から、後者の反応経路における反応物と中間体との間の遷移状態付近には、水素の転位とメチル基の転位が共存し、極めて興味深い遷移状態を形成していることが分かった。

Method of Calculation

We carried out all calculations on the basis of a hybrid Hartree–Fock/density functional theory (HF/DFT) method, using the Gaussian 94 ab initio program package.[28] We optimized local minima (on a potential energy hypersurface) corresponding to reactants, products, and intermediates using the Becke–Lee–Yang–Parr HF/DFT method (B3LYP).[29, 30] Sextet and quartet spin states were taken into consideration. The spin-unrestricted method was applied to such open-shell systems. We confirmed from $\langle S^2 \rangle$ values that no spin contamination was included in all calculations. We optimized the geometries of transition states (TSs) using the same method. Vibrational frequencies were systematically computed in order to ensure that, on a potential hypersurface, all optimized geometries correspond to a local minimum point which has all real frequencies or a saddle point which has only one imaginary frequency. Potential energy surfaces were calculated at the B3LYP/6-311G**//B3LYP/3-21G* level of theory. We carried out geometry optimizations with the 6-311G** basis set for the important intermediates $HO-Fe^+-CH_3$ and $H-Fe^+-OCH_3$ in both the spin states.

It is not necessarily obvious from the structure of the transition state or the orientation of the transition vector whether the transition state connects the desired reactants and products. In such cases, an analysis of the intrinsic reaction coordinate (IRC)[31, 32] is very useful in order to follow the reaction pathway from the transition state to the local minima, that is the reactants, intermediates, and products. As we will see, IRC analyses are found to be very effective for the determination of the true reaction pathways, since there appear to be several nontrivial transition states in this work.

We calculated IRCs in a mass-weighted internal coordinate system at the B3LYP level using the Gonzalez–Schlegel method[33] available in the Gaussian 94 program. IRC analyses coupled with the hybrid HF/DFT method were carried out with the 3-21G* basis set. We performed orbital interaction analyses with YAeHMOP (extended Hückel MO program package).[34] Hewlett Packard J200, 712, and Silicon Graphics R10000 workstations were used for calculations in this study.

Results and Discussion

Reaction Paths for Methane–Methanol Conversion: By means of calculational trial and error, we found two possible reaction paths for the methane–methanol conversion in which one intermediate and two transition states are included in each path, as indicated in Scheme 1. Thus, taking the sextet and quartet spin states into account, there are four reaction paths in this conversion. The reactant, product, and intermediates were calculated with a qualitative method,[18c] but we have no information about the transition states so far.

The first reaction path includes an insertion species, $HO-Fe^+-CH_3$, which both Schwarz and Armentrout proposed as playing an important role, as mentioned above. On the other hand, the second reaction path proceeds through a different intermediate, $H-Fe^+-OCH_3$. We call these reaction species

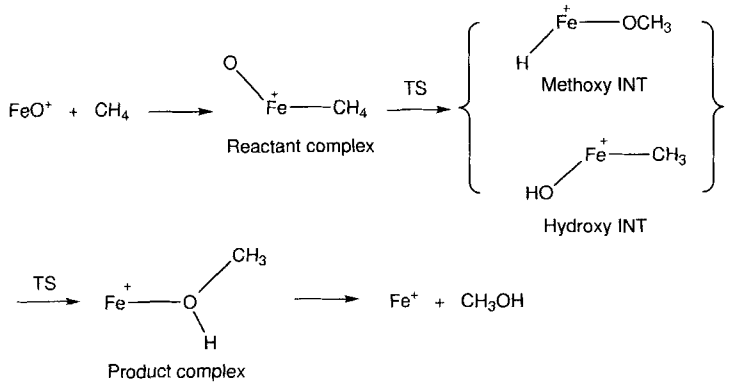

Scheme 1. The two reaction paths for the conversion of methane to methanol catalyzed by FeO^+.

hydroxy and methoxy intermediates throughout this paper. ECP–DZ calculations indicate that the hydroxy intermediate is more stable than the methoxy intermediate by 20 kcal mol^{-1}.[18c] However, since there is no information on the transition states, it is not possible to predict which is the more favorable reaction path. Although these reaction paths seem to be quite simple, the actual situation is rather more complicated.

The transition state connecting the reactant and the hydroxy intermediate, $HO-Fe^+-CH_3$, is associated with just a simple shift of hydrogen. On the other hand, both C–H bond cleavage and methyl migration occur in the transition state towards the methoxy intermediate, $H-Fe^+-OCH_3$. Our main concern in this paper is to discover, from the standpoint of the activation energy, whether the first reaction path (via the hydroxy intermediate) is more favorable than the second one (through the methoxy intermediate), as previously suggested.[18a–c] Thus, we need detailed information on these transition states. In the course of the entire reaction paths shown in Scheme 1, only elementary hydrogen- and methyl-shift reactions are assumed to occur. Moreover, we assume these reactions proceed in a concerted manner. We will analyze in detail the orbital interactions for the binding of methane to FeO^+, which is the most important and interesting initial stage for the activation of methane.

Reactant and Product Complexes: We define the reactant, transition states, intermediates, and product along the two reaction paths, as shown in Scheme 1. Let us look first at the reactant complex of FeO^+ and CH_4. The optimized geometries of the reactant in each spin state (sextet and quartet) are shown in Figure 1. These structures show that the coordination of methane occurs at the Fe atom, thus forming the interesting Fe–C bond. The bond angles for C-Fe-O are 142.3° and 109.4° in the sextet and quartet states, respectively. Moreover, the Fe–C bond length of 2.236 Å in the high-spin sextet state is longer than that of 2.092 Å in the low-spin quartet state. The Fe–O distance of the reactant in each spin state is about 1.6 Å; the Fe–O distance and the atomic (Mulliken) charge of the oxygen of ≈ -0.3 remain unchanged compared to those of free FeO^+ in each spin state. We confirmed, by means of vibrational analyses, that the geometries shown in Figure 1 correspond to true local minima on the potential energy hypersurfaces in these spin states.

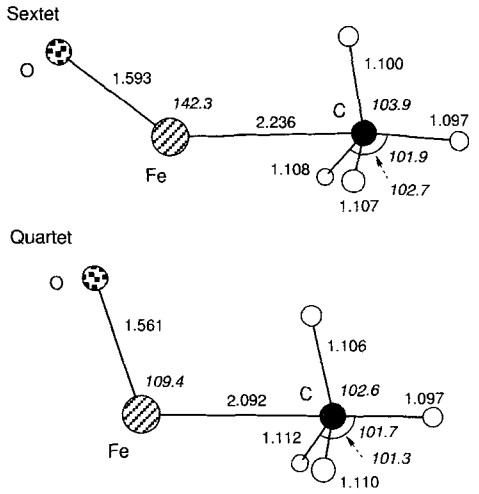

Figure 1. Calculated geometries of reactant complexes in the sextet and quartet states, with atomic distances [Å] and bond angles (*italic*) [°].

Let us now pay attention to the coordinated methane itself. In these reactant geometries, the three H–C–H angles of methane indicated in Figure 1 are decreased by 6.8–8.2° from 109.5° of the T_d-type methane. As a result, the coordinating methane adopts an almost C_{3v}-type geometry. This is an interesting calculational result for methane activation. It is important to note that all the C–H bond lengths of methane in these structures remain unchanged from a standard value. Shestakov and Shilov[35] have proposed that the activation of hydrocarbons proceeds through an interaction between an oxoferryl species and hydrocarbons. Their model postulates a C_{3v}-type deformation of the hydrocarbon at the initial stage of the reaction. This C_{3v}-type deformation was also proposed theoretically to occur in the coordination of methane to a supposed active center of methane monooxygenase (MMO) enzyme.[17] The optimized geometries for the reactant complex shown in Figure 1 strongly support these proposals.

As a consequence of a C_{3v}-type deformation of methane, one orbital, which comes from each threefold-degenerate t_2 and t_2^* orbital of methane, approaches the frontier orbital region (Scheme 2). The interaction between one orbital from the occupied t_2 and the d-block of ML_n complexes was found to be important for the activation of methane.[21] Billups et al.[36] also

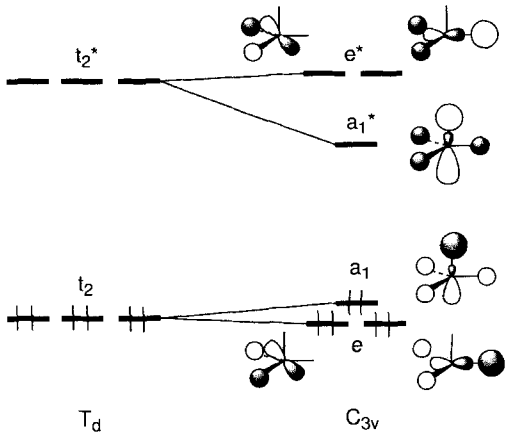

Scheme 2. Frontier orbitals of T_d- and C_{3v}-type methane.

0947-6539/97/0307-1162 $ 17.50+.50/0 Chem. Eur. J. 1997, 3, No. 7

suggested the C_{3v} deformation of methane from the low-temperature IR spectrum of $Co(CH_4)$, in which the triply degenerate absorption at 1305.3 cm^{-1} is split into two peaks.

We know from the Fe–C distances (2.236 and 2.092 Å in the sextet and quartet states, respectively) that the interaction between the iron and the carbon of the coordinating methane is not weak in the reactant complex. It is interesting that the atomic charge of the carbon in the reactant complex is −1.0 in both the spin states, but the total charge of the coordinating methane is +0.22 and +0.24 in the sextet and quartet states, respectively. Since the atomic charge of the carbon in free methane is −0.76 in this methodology, the carbon is more negatively charged in this complex. Thus, upon formation of the reactant complex, a charge transfer and a significant charge polarization occur in the coordinating methane. The electrostatic interactions, such as charge-induced dipole and quadrupole, are likely to play a role in the bonding of this interesting reactant complex.

Let us look at the orbital interaction between the FeO^+ and CH_4 fragments for the analysis of the methane activation. The binding of methane to FeO^+ is the most interesting aspect in the initial stage of the entire reactions for the conversion of methane to methanol. Figure 2 shows the fragment molecular orbital

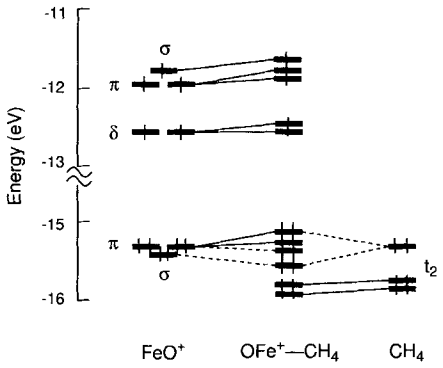

Figure 2. Fragment molecular orbital (FMO) analysis in the sextet state for $FeO^+ + CH_4 \rightarrow OFe^+-CH_4$. The threefold degenerate t_2 HOMO of T_d methane is split in the C_{3v}-type methane.

analysis, based on the extended Hückel method, for the formation of the OFe^+-CH_4 complex, in which the optimized B3LYP geometry in the sextet state, indicated in Figure 1, is used.

From the viewpoint of perturbation theory, two kinds of interactions play an essential role:[21] the interaction between the HOMO of the substrate and the LUMO of the ML_n complex, as well as that between the LUMO of the substrate and the HOMO of the complex. The two-orbital four-electron interaction between filled orbitals of substrate and complex is not important. There are orbital interactions between the upper t_2 of methane and the singly occupied π and σ d orbitals of FeO^+, which will result in a significant charge transfer. In fact, the total charge of the methane is +0.16 in extended Hückel calculations, which is consistent qualitatively with the B3LYP value of +0.22 and +0.24 in the sextet and quartet states, respectively. The C_{3v} deformation of methane plays an essential role in these orbital interactions, because, as a consequence of this deformation, one of the threefold-degenerate t_2 HOMOs goes up into the frontier orbital region. This is favorable for the orbital interactions from second-order perturbation theory. On the other hand, the t_2^* LUMOs of methane lie remarkably high at +3 ~ 5 eV, so that these unoccupied orbitals do not greatly contribute to the formation of the OFe^+-CH_4 complex.

Having described the formation of the Fe–C bond in the reactant complex, we shall next look at the product, which is a complex of Fe^+ and methanol (Scheme 1). The two geometries for the sextet and quartet states are quite similar, as shown in Figure 3. These were also confirmed to be local minima on each potential energy hypersurface by means of vibrational analyses. These structures correspond to a methanol molecule coordinating to Fe^+. The methanol moiety in these structures is quite similar to the optimized structure of methanol itself, except for the elongated C–O bond, as indicated.[18c] The fragmentation of the product complex, which leads to free methanol and Fe^+, is interesting.

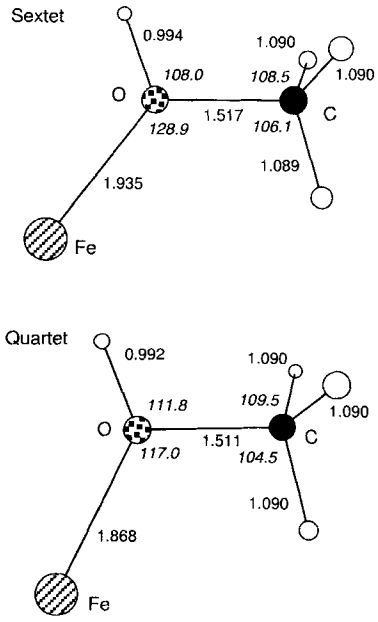

Figure 3. Calculatd geometries of product complexes in the sextet and quartet states with atomic distances [Å] and bond angles [°].

Intermediates and Transition States

Sextet Reaction Paths: In this section, we will discuss two possible reaction pathways for the sextet spin state. Let us look at the geometries of the two important intermediates, $HO-Fe^+-CH_3$ and $H-Fe^+-OCH_3$. These geometries in the sextet state are shown in Figure 4. We confirmed that these optimized geo-

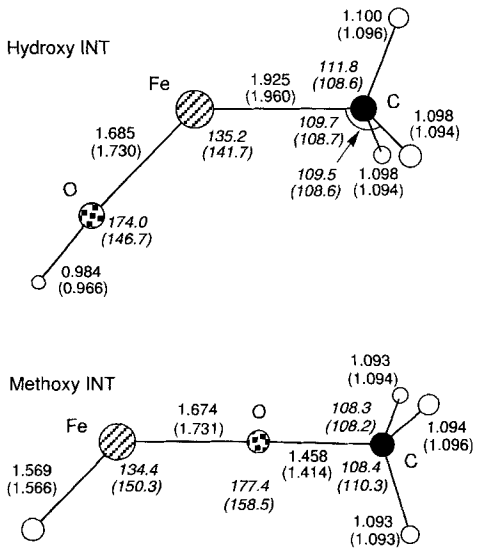

Figure 4. Calculated geometries of hydroxy and methoxy intermediates in the sextet state. Values in parentheses are those from 6-311G** calculations.

metries correspond to true local minima on the sextet potential energy surface. We would first like to consider the hydroxy intermediate. Schröder et al.[18c] used ECP–DZ calculations to show that this intermediate has a C_{3v} geometry in which the O–Fe and Fe–C bonds are colinear. In contrast, the B3LYP method predicted a bent form with an O-Fe-C angle of 135.2°. Moreover, the Fe–C distance of 1.925 Å in the B3LYP geometry is much shorter than that of 2.515 Å in the ECP–DZ geometry. The Fe–O bond length is 1.685 Å in the B3LYP calculation. Since the total charge of the O–H group is almost neutral, −0.19, this short distance seems to be reasonable. The three Fe-C-H bond angles are close to 109.5°, those of methane. A methyl shift in this intermediate is thought to give the final product.

The structure of the methoxy intermediate, $H-Fe^+-OCH_3$, in the sextet state, was also reported in ref. [18c]. Here the C–O, O–Fe, and Fe-H bonds were proposed to be colinear. However, our calculations gave the most stable O–Fe–H bond angle as 134.4°. This is not an important difference, but the bent form seems to be a realistic structure for this intermediate from our vibrational analyses. Moreover, the Fe–O distance of 1.674 Å in the B3LYP geometry is in remarkable contrast to that of 2.157 Å in the ECP–DZ geometry. Since the total charge of the OCH_3 moiety is nearly zero (− 0.09), our optimized Fe–O distance of 1.674 Å is quite reasonable. We believe that our geometry optimizations were correctly carried out, because $\langle S^2 \rangle$ values indicate no spin contamination included in these states. One can imagine that this intermediate may also be converted directly into the final product by a simple hydrogen migration.

The hydroxy intermediate is more stable than the methoxy one by 20.4 kcal mol^{-1}, which is consistent with the ECP–DZ result.[18c] The hydroxy intermediate is extremely stable; it is 2.3 kcal mol^{-1} more stable than the final product and 21.4 kcal mol^{-1} more stable than the reactant complex. However, this fact does not immediately imply that the hydroxy intermediate plays an important role in the entire methane–methanol conversion in the gas phase. It is therefore important to know the activation energies from the reactant to these intermediates and those from the intermediates to the final product.

In Figure 5, we propose the entire reaction pathways via the two kinds of intermediates described above. A possible reaction path from the reactant to the hydroxy intermediate, $HO-Fe^+-CH_3$, via TS1, is also included. This process consists of a simple hydrogen shift from the coordinating methane to the oxygen, and proceeds through a typical four-centered transition state. This intermediate is subsequently converted into the final product through a simple [1,2]-methyl migration to the oxygen. Transition state TS2 links the hydroxy intermediate to the final product and has a trivial three-centered structure. One can easily imagine the structure of this transition state by looking at those of the intermediate and product.

We propose a different reaction pathway connecting the reactant and product via the methoxy intermediate, $H-Fe^+-OCH_3$. In our reaction scheme, this intermediate is formed directly from the reactant by hydrogen- and methyl-shift reactions in the sextet state, as indicated. A key point in this reaction is the almost simultaneous occurrence of the hydrogen shift and the [1,2]-migration of the methyl group. The structure of the four-centered transition state, TS3, seems to be quite reasonable both for the cleavage of C–H bond and for the migration of a methyl group. IRC analysis is very important for the characterization of this reaction path, since we cannot intuitively judge whether or not the transition state we found is the true one connecting the reactant and intermediate. This is a two-step reaction, but it looks like a single step because the associated two transition states are located in the same region of space on the sextet potential energy surface, as described later. The methoxy intermediate is converted into the final product through a simple [1,2]-hydrogen shift from the iron to the oxygen. TS4, connecting the methoxy intermediate and the final product, has a typical, three-centered structure. In contrast to TS3, the structure of TS4 is trivial, and one can easily imagine the structure of this transition state in view of the methoxy intermediate and the final product.

The two main reaction paths through the two important intermediates, $HO-Fe^+-CH_3$ and $H-Fe^+-OCH_3$, are outlined in Figure 5. As we will see later, the reaction paths in the quartet state are quite similar to these.

Having described the outline of the reactions, let us now turn our attention to the geometries of the transition states. We found two transition states along each reaction path, as indicated in Figure 5. We would like to look at the first reaction path (in the sextet spin state), which proceeds through the hydroxy intermediate, $HO-Fe^+-CH_3$. The structures of TS1(s) and TS2(s) in the course of this reaction path are shown in Figure 6, in which TS1(s) represents TS1 in the sextet state. Vibrational analyses indicated that these transition-state structures have only one imaginary frequency mode, which ensures that these correspond to a saddle point on the sextet potential energy surface. The transition vectors leading to the forward reaction and the corresponding imaginary frequencies are also indicated in Figure 6.

TS1(s) corresponds to a simple hydrogen shift which leads the reactant to the hydroxy intermediate, $HO-Fe^+-CH_3$. Thus, the C–H bond length of 1.456 Å and the O–H bond length of 1.355 Å in the bond-cleavage and -creation region are quite reasonable. The Fe–O and Fe–C distances of

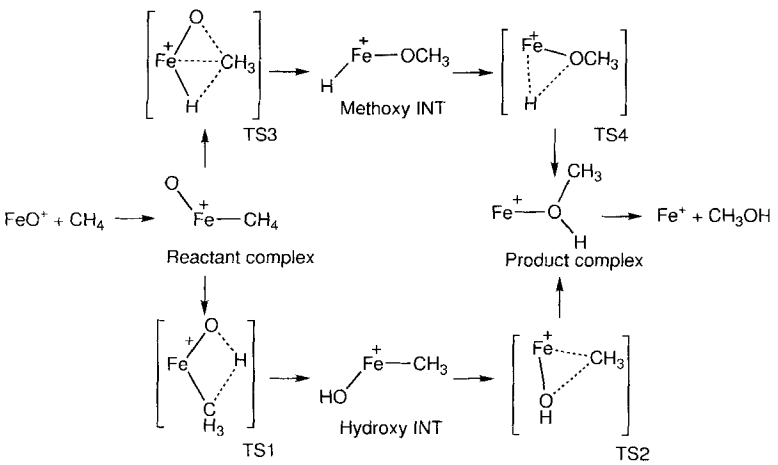

Figure 5. Two reaction paths, via hydroxy or methoxy intermediates, for the conversion of methane to methanol catalyzed by FeO^+.

0947-6539/97/0307-1164 $ 17.50+.50/0 Chem. Eur. J. 1997, 3, No. 7

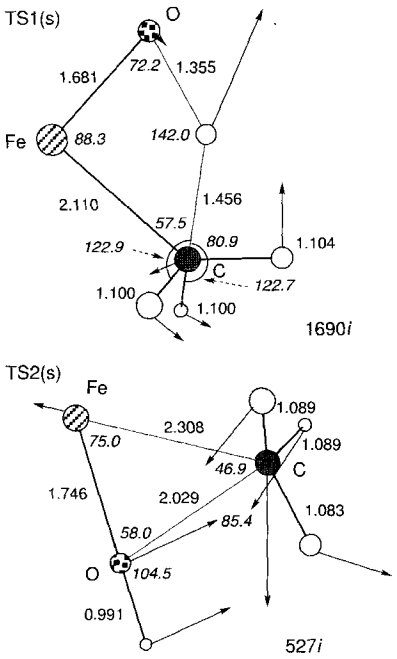

Figure 6. Calculated geometries for TS1(s) and TS2(s) on the hydroxy-intermediate path in the sextet state. Imaginary vibrational modes (transition vectors) for the forward reactions are given in cm^{-1}.

1.681 Å and 2.110 Å respectively in TS1(s) are slightly longer than those of the reactant. Although the Fe–O distance remains almost unchanged during this hydrogen shift, the Fe–C distance shortens remarkably after passing TS1(s), as indicated in the geometry of the hydroxy intermediate shown in Figure 4. TS2(s) connects the hydroxy intermediate and the final product by a methyl migration. The Fe–O distance changes from 1.685 Å in the hydroxy intermediate to 1.935 Å in the final product during this migration. The Fe–O distance of 1.746 Å in TS2(s) is thus an intermediate value. The transition-state structures of TS1(s) and TS2(s) have typical four- and three-centered structures (Figure 6).

Let us look next at the transition states along the second reaction path in the sextet state. TS3(s) connects the reactant and the methoxy intermediate, $H-Fe^{+}-OCH_3$ (Figure 5), and it is at the mid-point for both the hydrogen shift from the methane to the iron and the methyl shift from the iron to the oxygen. TS3(s) is very intriguing because two basic reactions are related to it, as mentioned above. In contrast to TS1(s), it was difficult to obtain the structure of TS3(s) from those of the reactant and intermediate, because both C–H bond cleavage and migration of the methyl group occur simultaneously in this reaction. Although we inspected the potential energy surface very carefully, a stable point was not found in the vicinity of this transition state. Thus, we can reasonably treat TS3(s) as a single transition state. The optimized geometries for TS3(s) and TS4(s) are shown in Figure 7.

The Fe–C distance in TS3(s) (1.981 Å) is rather short compared to that in the reactant. The dissociating C–H bond length is 2.624 Å. Although TS3(s) is associated with both a hydrogen shift and a methyl migration, we find that in the vicinity of this transition state the cleavage of the C–H bond is completed earlier than the methyl shift. This is also seen from the Fe–H distance of 1.551 Å in TS3(s), which is rather short for the transition state geometry associated with Fe–H bond cleavage or formation. We will see, from a detailed IRC inspection, that two transition states, caused by the hydrogen shift and the methyl migration, are overlapping in the same region of the potential energy surface. The former transition state (hydrogen shift) is screened by the latter one (methyl migration). Figure 7 also shows the optimized geometry of TS4(s), which links the

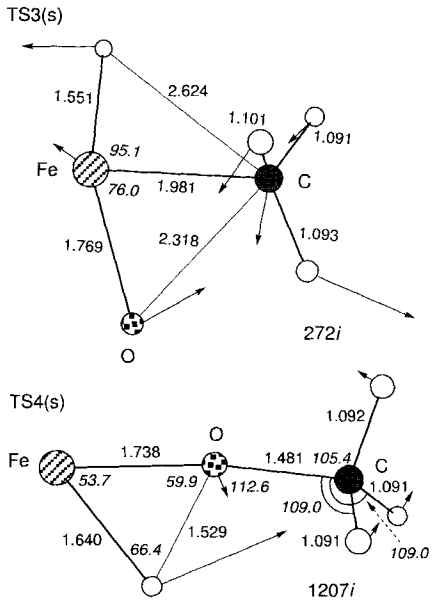

Figure 7. Calculated geometries for TS3(s) and TS4(s) on the methoxy-intermediate path in the sextet state.

methoxy intermediate to the final product. TS4(s) has a trivial transition-state structure lying between the methoxy intermediate and the final product—a typical three-centered structure that corresponds to a simple [1,2]-hydrogen shift.

In Figure 8 we show the energy diagram along the entirety of the reaction pathways, as well as the structures of the minima

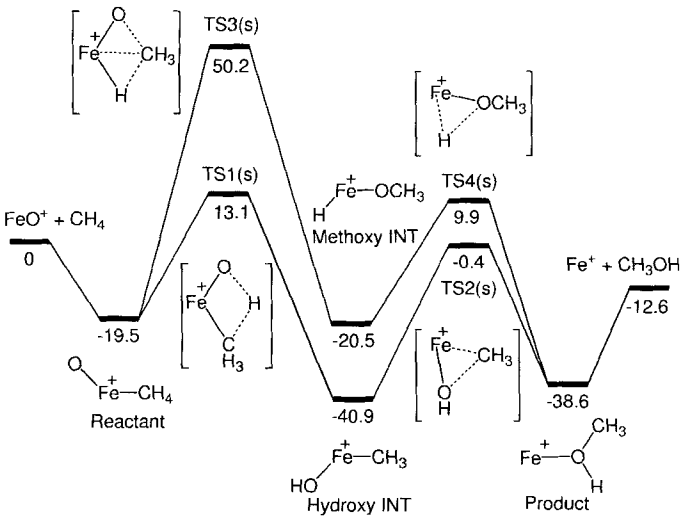

Figure 8. Potential energy diagram in the sextet state for the conversion of methane to methanol. Relative energies are given in kcal mol^{-1}.

and saddle points in the sextet spin state. What can we predict from this energy diagram? First of all, the reactant is stabilized compared with FeO^{+} and CH_4 by 19.5 kcal mol^{-1}, due to the formation of Fe–C bond. The formation of this bond and the five-coordinate methane are theoretically very interesting, and in the previous section we looked at the fragment molecular orbital analysis on the complex formation of FeO^{+} and methane.

The activation energy from the reactant to the hydroxy intermediate, $HO-Fe^+-CH_3$, is 32.6 kcal mol^{-1}; on the other hand, that from the reactant to the methoxy intermediate, $H-Fe^+-OCH_3$, is very high (69.7 kcal mol^{-1}) in the sextet state. The difference between the energies of $HO-Fe^+-CH_3$ calculated at the B3LYP/6-311G**//B3LYP/3-21G* and B3LYP/6-311G** levels is only 2.3 kcal mol^{-1} and that between the energies of $H-Fe^+-OCH_3$ at the same levels is 2.5 kcal mol^{-1} because these 3-21G* and 6-311G** geometries are similar to each other (Figure 4). The hydroxy intermediate is more stable than the methoxy intermediate by 20.4 kcal mol^{-1}. Moreover, it is noted that the hydroxy intermediate is stable compared to the reactant and product. Therefore, from an energetic viewpoint, we conclude that the hydroxy intermediate is easily formed and that the reaction path toward this intermediate is energetically preferred on the sextet potential energy surface.

However, the activation energy from the hydroxy intermediate to the final product is large, 40.5 kcal mol^{-1}, because the hydroxy intermediate is stable, as mentioned above. On the other hand, that from the methoxy intermediate to the final product is 30.4 kcal mol^{-1}. On considering the total of the two activation energies in each path, we can predict that the reaction path through the hydroxy intermediate is more favorable for the entire methane–methanol conversion in the sextet state.

Quartet Reaction Paths: The reaction pathways in the quartet state are quite similar to those in the sextet state. We have also found the hydroxy and methoxy intermediates in the quartet state. Let us first look at the transition states towards these important insertion intermediates. Figure 9 depicts the transition state towards the hydroxy intermediate, TS1(q), and the transition state towards the methoxy intermediate, TS3(q). Here TS1(q) represents TS1 in the quartet state. Vibrational analyses indicated that these transition-state structures have only one imaginary frequency mode. The transition vectors leading to the forward reaction and the corresponding imaginary frequencies are also indicated in Figure 9.

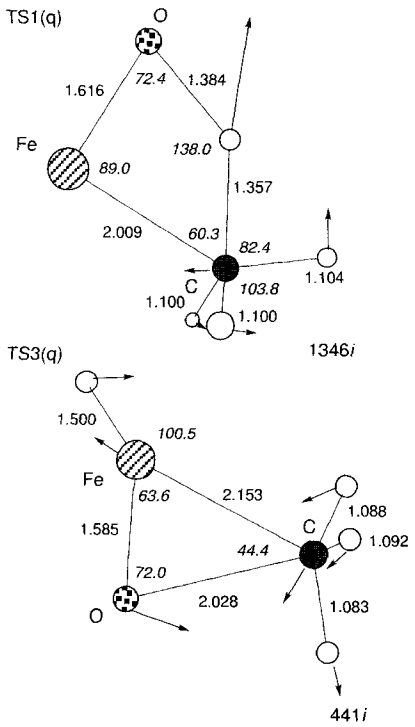

Figure 9. Calculated geometries of TS1(q) and TS3(q) in the quartet state. Imaginary vibrational modes for the transition states are given in cm^{-1}.

The geometry of TS1(q) is quite similar to that of TS1(s) in Figure 6. These transition states correspond to a hydrogen shift that links the reactant and the hydroxy intermediate. Thus, the C–H bond length of 1.357 Å and the O–H bond length of 1.384 Å in the bond-cleavage and -creation region are reasonable. The geometry of TS3(q) is essentially similar to that of TS3(s); however, since the O-Fe-H angle is larger in TS3(q), these two transition states have a different shape.

We look next at the hydroxy and methoxy intermediates in the quartet spin state. The geometries of these species in the quartet state are shown in Figure 10. Let us first compare the sextet and quartet geometries of the hydroxy intermediate, $HO-Fe^+-CH_3$. Although the bond lengths of these are quite similar, the bond angles are very different. As shown in Figures 4 and 10, the C-Fe-O and Fe-O-H angles in the sextet state are 135.2° and 174.0°, respectively; in contrast, those in the quartet state are 107.6° and 138.2°, respectively. Generally speaking, the low-spin quartet state seems to prefer a bent geometry in this system. This is also true in the methoxy intermediate, $H-Fe^+-OCH_3$. The C-O-Fe and O-Fe-H angles in the sextet state are 177.4° and 134.4°, respectively; on the other hand, those in the quartet state are 142.0° and 106.0°, respectively. All these bond angles are, in general, smaller in the quartet state than in the sextet state. This point is interesting, considering that low-spin methylene prefers a bent geometry compared to high-spin methylene.[37] We believe the present calculational results to be correct, because there is no spin contamination in either of the spin states.

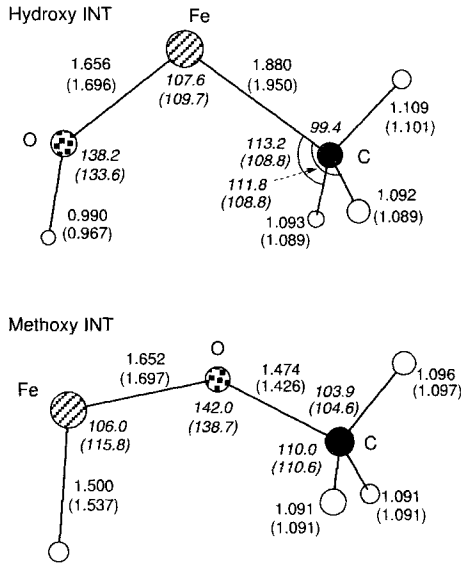

Figure 10. Calculated geometries of hydroxy and methoxy intermediates in the quartet state. Values in parentheses are those from 6-311G** calculations.

The hydroxy intermediates of the quartet and sextet states are shown to be of nearly equal energy by B3LYP calculations. The ground state of an analogous insertion species, $H-Fe^+-OH$, formed by the reaction of $FeO^+ + H_2$ in the gas phase, has been

0947-6539/97/0307-1166 $ 17.50+.50/0 Chem. Eur. J. 1997, 3, No. 7

calculated as a quartet.[18d] The methoxy intermediate of the quartet state lies 4.6 kcal mol^{-1} above that of the sextet state.

Having described the two important intermediates, we next take a look at the transition states towards the final product along the two quartet reaction paths. Figure 11 shows the geometries for these two transition states. The transition vectors

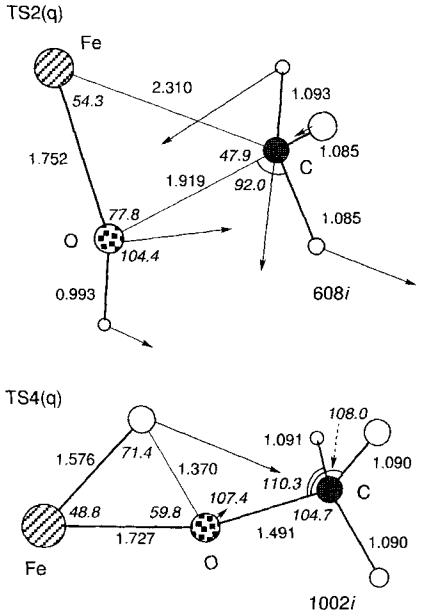

Figure 11. Calculated geometries of TS2(q) and TS4(q) in the quartet state.

point exactly towards the formation of the final product. These are associated with typical [1,2]-methyl and -hydrogen migrations which proceed through typical three-centered transition states. These geometries are very similar to those of the sextet state.

The energy diagram along the entire reaction pathways, as well as the optimized geometries at minima and saddle points on the quartet potential energy surface, are shown in Figure 12. These relative energies, in units of kcal mol^{-1}, are measured

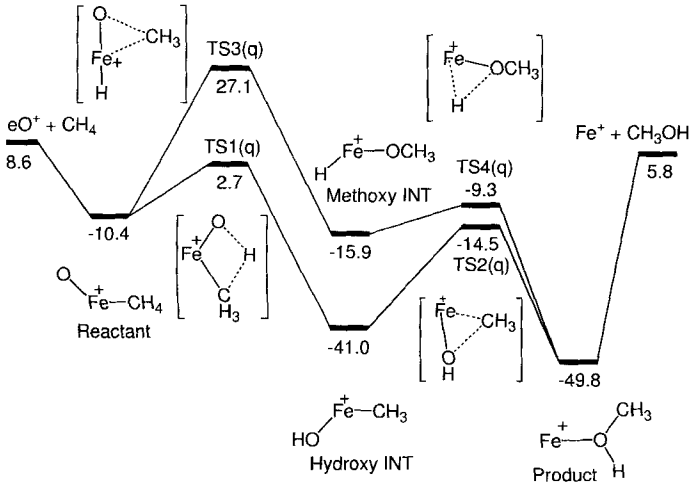

Figure 12. Potential energy diagram in the quartet state for the conversion of methane to methanol. Relative energies, measured from $FeO^+ + CH_4$ in the sextet state, are given in kcal mol^{-1}.

from the energy of $FeO^+ + CH_4$ in the sextet state (see Figure 8). The quartet state of FeO^+ is calculated to be 8.6 kcal mol^{-1} higher than that of the sextet state. Carter and Goddard[38] and Fiedler et al.[39] calculated the high-spin and low-spin states of several transition metal oxides, MO^+, using the generalized valence bond (GVB) and CASSCF methods, respectively. The calculated energy splitting between the sextet and quartet Fe^+ (18.4 kcal mol^{-1}) clearly overestimates the experimental value of 6.4 kcal mol^{-1}.[40] Although it is theoretically clear that such multiconfiguration approaches offer a reasonable and satisfying treatment for highly degenerate Fe^+ and FeO^+, the present hybrid HF/DFT method is found to behave fairly well for Fe^+ and FeO^+ in both spin states.

The energy differences between the intermediates and the transition states are relatively small in the quartet state. We think this is partly due to the fact that the reactant and intermediates prefer bent geometries in the quartet state, compared to those in the sextet state, as mentioned above. The bent geometries in the quartet state would be favorable for the formation of three- and four-centered transition states.

The reactant complex in the quartet state lies 9.1 kcal mol^{-1} above that in the sextet state. The activation energy from the reactant to the hydroxy intermediate is therefore not large, 13.1 kcal mol^{-1}. On the other hand, that from the reactant to the methoxy intermediate is 37.5 kcal mol^{-1}. The difference between the energies of $HO-Fe^+-CH_3$ calculated at the B3LYP/6-311G**//B3LYP/3-21G* and B3LYP/6-311G** levels is only 2.7 kcal mol^{-1} and that between the energies of $H-Fe^+-OCH_3$ at the same levels is 2.2 kcal mol^{-1}. The result is because these 3-21G* and 6-311G** geometries are similar to each other, as shown in Figure 10. Therefore, the reaction path via the hydroxy intermediate is also more favorable in the quartet state. We can see that the potential curve in the diagram of the quartet state is relatively flat. Thus, these reactions are predicted to occur easily in the quartet state.

The hydroxy intermediate lies below the methoxy intermediate by 25.1 kcal mol^{-1} in the quartet state. This energy difference is comparable to 25.7 kcal mol^{-1} for that in the sextet state. Consequently, the activation energy from the hydroxy intermediate to the final product is 26.5 kcal mol^{-1}, and that from the methoxy intermediate to the product is 6.6 kcal mol^{-1}.

The potential curves of the quartet state are flat compared with those of the sextet state. Therefore, crossing between the high-spin and low-spin potential energy hypersurfaces can occur, as suggested by Schwarz's and Armentrout's groups.[18, 19] As discussed in ref. [18h], an analysis of the spin–orbit coupling is essential, along with that of barrier heights, because a curve crossing between high-spin and low-spin states may constitute a distinct mechanistic step along these reaction coordinates. The comparison of two-state reactivity with single-state reactivity in H–H and C–H bond activation catalyzed by bare oxocations, MO^+, has already been described.[18h] In any case, energetic factors such as activation energy play an essential role, so that the sextet and quartet state energy diagrams we show in Figures 8 and 12 will contribute greatly to the analysis of the methane–methanol conversion.

Intrinsic Reaction Coordinates: IRC analyses were carried out along the entire reaction pathways for both the spin states. The

IRC analyses confirmed that the intermediates and transition states we have shown so far are exactly on the true reaction paths from the reactant to the final product in the sextet and quartet spin states. In particular, we are interested in the analyses of the first half of the reaction pathways, that is prior to the formation of the hydroxy and methoxy intermediates, because the second half of the reactions are quite trivial, as already demonstrated. In this section, we describe IRC analyses for the reaction pathways towards the hydroxy and methoxy intermediates in the sextet state. These are rather complicated and nontrivial compared to those from the intermediates to the final product.

IRCs in Sextet State: Let us look first at the reaction path towards the hydroxy intermediate in the sextet state. Figure 13

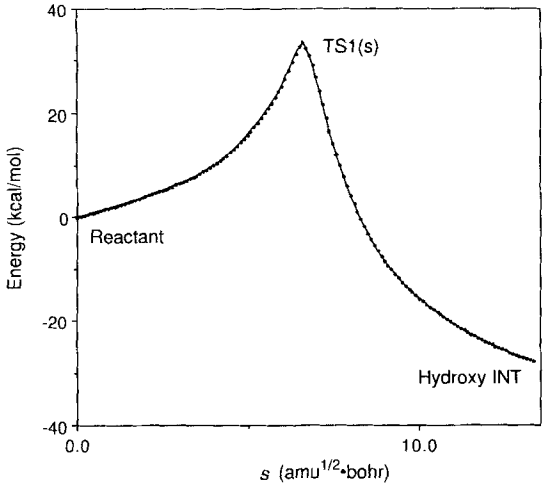

Figure 13. Energy profile along the IRC from the reactant to the hydroxy intermediate in the sextet state.

shows the energy profile along the IRC from the reactant to the hydroxy intermediate. This is a typical energy profile due to a single transition state. TS 1(s) corresponds to the hydrogen shift from the coordinating methane to the oxygen, as indicated in Figure 6. Since this peak is very sharp, the IRC is easy to calculate.

We next consider the interesting reaction path towards the methoxy intermediate. As shown in Figure 14, the energy profile is asymmetric, because TS 3(s) is composed of the two transition states, as mentioned above. One of these corresponds to a hydrogen shift, and the other to a methyl shift (Figure 7). The hydrogen shift occurs earlier and this energy peak is covered by the second peak of the methyl migration, which occurs later. Interestingly, these two transition states coexist in the same region of the potential energy surface, so that the overlap of these peaks leads to an asymmetric single peak. We do not think it is a problem to treat this as an ordinary single peak. In fact, a close inspection of the potential energy surface confirmed that there is no stable intermediate in the vicinity of this reaction path.

Detailed analyses of the change in the bond lengths and angles, as well as the energy profiles along the IRCs of the methane–methanol conversion, will be reported elsewhere.

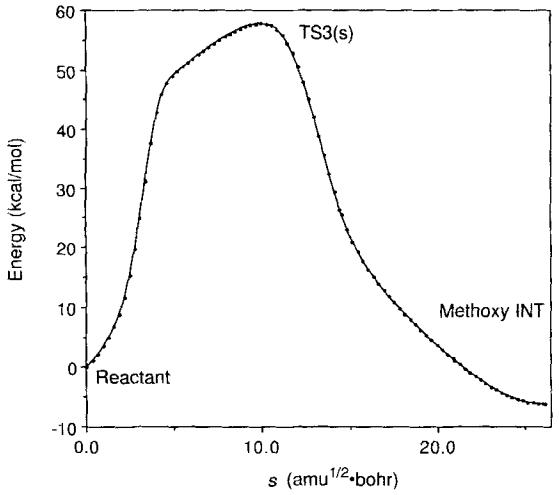

Figure 14. Energy profile along the IRC from the reactant to the methoxy intermediate in the sextet state. The main peak is due to methyl migration and the shoulder due to the hydrogen shift which is completed sooner.

Summary and Conclusions

We have used a modern hybrid HF/DFT method to describe the theoretical conversion of methane to methanol catalyzed by FeO^+ in the gas phase. The geometries of the reactants, products, intermediates, and transition states along the two reaction pathways via the important insertion intermediates, $HO-Fe^+-CH_3$ and $H-Fe^+-OCH_3$, have been described in both the sextet and quartet spin states. The energy profiles of the quartet reaction pathways are rather flat compared to the sextet ones. On the basis of the activation energies we have calculated, we conclude that the reaction path via the hydroxy intermediate is preferred for both spin states. These calculational results are fully consistent with an experimental prediction that the hydroxy intermediate is a major intermediate.[18a, b] We have not discussed a possible cross over between the high-spin and low-spin potential energy hypersurfaces. Since this effect is thought to play an important role in the reactions catalyzed by transition-metal oxides,[18h] we will consider this interesting problem in future studies.

We believe that our theoretical study on the possible reaction pathways for the conversion of methane to methanol will also be useful for the analysis of catalytic and enzymatic functions of C–H and C–C bond activation by iron complexes. In particular, our study may be useful for the elucidation of the catalytic functions of cytochrome P-450 and methane monooxygenase (MMO), since they contain oxoferryl species, Fe–O, in their catalytically active centers. The activation energies along the possible reaction pathways we have shown are rather small compared to the C–H bond energy of ≈ 100 kcal mol^{-1}. We think that the proposed concerted mechanisms may play a role in such metalloenzyme systems, although at present we cannot easily compare simple gas-phase reactions and complicated enzymatic reactions. In a previous paper,[17] Yoshizawa, Yamabe, and Hoffmann discussed the importance of the C_{3v}-type deformation of methane in the initial stage of methane activation in the catalytic cycle of MMO. In this paper, our ab initio calculations have shown that C_{3v} deformation of methane plays a role in

0947-6539/97/0307-1168 $ 17.50+.50/0 Chem. Eur. J. 1997, 3, No. 7

the formation of the OFe^+-CH_4 complex, which contains five-coordinate methane; we have clarified several aspects of the reaction pathways for the methane–methanol conversion catalyzed by FeO^+.

Acknowledgments: K. Y. is very grateful to Prof. R. Hoffmann of Cornell University for fruitful discussions on methane activation. K. Y. also thanks Drs. N. Goldberg (Cornell), D. Schröder (Berlin), and E. Merschrod (Cornell) for useful discussions and comments. We thank Dr. A. Fiedler (Okazaki) for useful suggestions on the calculations of transition-metal oxides. We are grateful for a Grant-in-Aid for Scientific Research from the Ministry of Education, Science and Culture of Japan and to the Japan Society for the Promotion of Science (JSPS-RFTF 96P00206) for their support of this work.

Received: October 9, 1996 [F487]

[1] A. E. Shilov, *The Activation of Saturated Hydrocarbons by Transition-metal Complexes*, D. Reidel, Dordrecht, **1984**.
[2] a) R. G. Bergman, *Science* **1984**, *223*, 902; b) B. A. Arndtsen, R. G. Bergman, T. A. Mobley, T. H. Peterson, *Acc. Chem. Res.* **1995**, *28*, 154.
[3] *Activation and Functionalization of Alkanes* (Ed.: C. L. Hill), Wiley, New York, **1989**.
[4] J. A. Davies, P. L. Watson, J. F. Liebman, A. Greenberg, *Selective Hydrocarbon Activation*, VCH, New York, **1990**.
[5] a) R. H. Crabtree, *The Organometallic Chemistry of the Transition Metals*, Wiley, New York, **1994**; b) R. H. Crabtree, *Chem. Rev.* **1985**, *85*, 245; c) R. H. Crabtree, *ibid.* **1995**, *95*, 987.
[6] H. D. Gesser, N. R. Hunter, C. B. Prakash, *Chem. Rev.* **1985**, *85*, 237.
[7] J. H. Lunsford, *Angew. Chem. Int. Ed. Engl.* **1995**, *34*, 970.
[8] J. J. Schneider, *Angew. Chem. Int. Ed. Engl.* **1996**, *35*, 1068.
[9] P. R. Ortiz de Montellano, *Cytochrome P-450: Structure, Mechanism, and Biochemistry*, Plenum, New York, **1986**.
[10] a) I. Bertini, H. B. Gray, S. J. Lippard, J. S. Valentine, *Bioinorganic Chemistry*, University Science Books, California, **1994**; b) S. J. Lippard, J. M. Berg, *Principles of Bioinorganic Chemistry*, University Science Books, California, **1994**.
[11] A. L. Feig, S. J. Lippard, *Chem. Rev.* **1994**, *94*, 759.
[12] J. D. Lipscomb, *Annu. Rev. Microbiol.* **1994**, *48*, 371.
[13] L. Que, Jr. in *Bioinorganic Catalysis* (Ed.: J. Reedijk), Marcel Dekker, New York, **1993**.
[14] W. Kaim, B. Schwederski, *Bioinorganic Chemistry*, Wiley, Chichester, **1994**.
[15] a) A. C. Rosenzweig, C. A. Frederick, S. J. Lippard, P. Nordlund, *Nature* **1993**, *366*, 537; b) A. C. Rosenzweig, P. Nordlund, P. M. Takahara, C. A. Frederick, S. J. Lippard, *Chem. Biol.* **1995**, *2*, 409.
[16] K. Yoshizawa, R. Hoffmann, *Inorg. Chem.* **1996**, *35*, 2409.
[17] K. Yoshizawa, T. Yamabe, R. Hoffmann, *New J. Chem.* **1997**, *21*, 151.
[18] a) D. Schröder, H. Schwarz, *Angew. Chem. Int. Ed. Engl.* **1990**, *29*, 1433; b) H. Schwarz, *ibid.* **1991**, *30*, 820; c) D. Schröder, A. Fiedler, J. Hrušák, H. Schwarz, *J. Am. Chem. Soc.* **1992**, *114*, 1215; d) A. Fiedler, D. Schröder, S. Shaik, H. Schwarz, *ibid.* **1994**, *116*, 10734; e) D. Schröder, H. Schwarz, *Angew. Chem. Int. Ed. Engl.* **1995**, *34*, 1973; f) R. Wesendrup, C. A. Schalley, D. Schröder, H. Schwarz, *Chem. Eur. J.* **1995**, *1*, 608; g) M. C. Holthausen, A. Fielder, H. Schwarz, W. Koch, *Angew. Chem. Int. Ed. Engl.* **1995**, *34*, 2282; h) S. Shaik, D. Danovich, A. Fiedler, D. Schröder, H. Schwarz, *Helv. Chim. Acta* **1995**, *78*, 1393; i) A. Fiedler, D. Schröder, H. Schwarz, B. L. Tjelta, P. B. Armentrout, *J. Am. Chem. Soc.* **1996**, *118*, 5047.
[19] a) N. Aristov, P. B. Armentrout, *J. Phys. Chem.* **1987**, *91*, 6178; b) L. S. Sunderlin, P. B. Armentrout, *ibid.* **1988**, *92*, 1209; c) R. Geoorgiadis, P. B. Armentrout, *ibid.* **1988**, *92*, 7060; d) P. B. Armentrout, J. L. Beauchamp, *Acc. Chem. Res.* **1989**, *22*, 315; e) P. A. M. van Koppen, J. Brodbelt-Lustig, M. T. Bowers, D. V. Dearden, J. L. Beauchamp, E. R. Fisher, P. B. Armentrout, *J. Am. Chem. Soc.* **1990**, *112*, 5663; f) P. A. M. van Koppen, J. Brodbelt-Lustig, M. T. Bowers, D. V. Dearden, J. L. Beauchamp, E. R. Fisher, P. B. Armentrout, *ibid.* **1991**, *113*, 2359; g) D. E. Clemmer, N. Aristov, P. B. Armentrout, *J. Phys. Chem.* **1993**, *97*, 544; h) Y.-M. Chen, D. E. Clemmer, P. B. Armentrout, *J. Am. Chem. Soc.* **1994**, *116*, 7815; i) D. E. Clemmer, Y.-M. Chen, F. A. Kahn, P. B. Armentrout, *J. Phys. Chem.* **1994**, *98*, 6522.
[20] T. C. Jackson, D. B. Jacobson, B. S. Freiser, *J. Am. Chem. Soc.* **1984**, *106*, 1252.
[21] a) J.-Y. Saillard, R. Hoffmann, *J. Am. Chem. Soc.* **1984**, *106*, 2006; b) R. Hoffmann, *Rev. Mod. Phys.* **1988**, *60*, 601.
[22] a) J. J. Low, W. A. Goddard III, *J. Am. Chem. Soc.* **1984**, *106*, 8321; b) J. J. Low, W. A. Goddard III, *ibid.* **1986**, *108*, 6115; c) J. K. Perry, G. Ohanessian, W. A. Goddard III, *J. Phys. Chem.* **1993**, *97*, 5238.
[23] a) M. R. A. Blomberg, U. Brandemark, P. E. M. Siegbahn, *J. Am. Chem. Soc.* **1983**, *105*, 5557; b) M. R. A. Blomberg, P. E. M. Siegbahn, U. Nagashima, J. Wennerberg, *ibid.* **1991**, *113*, 424; c) M. R. A. Blomberg, P. E. M. Siegbahn, M. Svensson, *ibid.* **1992**, *114*, 6095; d) P. E. M. Siegbahn, M. R. A. Blomberg, *Organometallics* **1994**, *13*, 354; e) P. E. M. Siegbahn, *ibid.* **1994**, *13*, 2833; f) P. E. M. Siegbahn, *J. Am. Chem. Soc.* **1996**, *118*, 1487; g) P. E. M. Siegbahn, R. H. Crabtree, *ibid.* **1996**, *118*, 4442.
[24] a) T. Ziegler, V. Tschinke, A. D. Becke, *J. Am. Chem. Soc.* **1987**, *109*, 1351; b) T. Ziegler, V. Tschinke, L. Fan, A. D. Becke, *ibid.* **1989**, *111*, 9177; c) T. Ziegler, E. Folga, A. Berces, *ibid.* **1993**, *115*, 636.
[25] a) N. Koga, K. Morokuma, *J. Phys. Chem.* **1990**, *94*, 5454; b) N. Koga, K. Morokuma, *J. Am. Chem. Soc.* **1993**, *115*, 6883; c) D. G. Musaev, N. Koga, K. Morokuma, *J. Phys. Chem.* **1993**, *97*, 4064; d) D. G. Musaev, K. Morokuma, N. Koga, K. Ngyen, M. S. Gordon, T. R. Cundari, *ibid.* **1993**, *97*, 11435; e) D. G. Musaev, K. Morokuma, *ibid.* **1994**, *101*, 10697; f) D. G. Musaev, K. Morokuma, *ibid.* **1996**, *100*, 11600.
[26] a) S. Sakaki, M. Ieki, *J. Am. Chem. Soc.* **1991**, *113*, 5063; b) S. Sakaki, M. Ieki, *ibid.* **1993**, *115*, 2373.
[27] a) T. R. Cundari, *J. Am. Chem. Soc.* **1992**, *114*, 10557; b) T. R. Cundari, M. S. Gordon, *ibid.* **1993**, *115*, 4210; c) T. R. Cundari, *ibid.* **1994**, *116*, 340.
[28] M. J. Frisch, G. W. Trucks, H. B. Schlegel, W. P. M. Gill, B. G. Johnson, M. A. Robb, J. R. Cheeseman, T. A. Keith, G. A. Patterson, J. A. Montgomery, K. Reghavachari, M. A. Al-Laham, V. G. Zakrzewski, J. V. Ortiz, J. B. Foresman, J. Cioslowski, B. B. Stefanov, A. Nanayakkara, M. Challacombe, C. Y. Peng, P. Y. Ayala, W. Chen, M. W. Wong, J. L. Andres, E. S. Replogle, R. Gomperts, R. L. Martin, D. J. Fox, J. S. Binkley, D. J. Defrees, J. Baker, J. J. P. Stewart, M. Head-Gordon, C. Gonzalez, J. A. Pople, *Gaussian 94*, Gaussian, Pittsburgh, Pennsylvania, **1995**.
[29] A. D. Becke, *Phys. Rev.* **1988**, *A38*, 3098.
[30] C. Lee, W. Yang, R. G. Parr, *Phys. Rev.* **1988**, *B37*, 785.
[31] a) K. Fukui, *J. Phys. Chem.* **1970**, *74*, 4161; b) K. Fukui, *Acc. Chem. Res.* **1981**, *14*, 363.
[32] *The Reaction Path in Chemistry: Current Approaches and Perspectives* (Ed.: D. Heidrich), Kluwer Academic, Dordrecht, **1995**.
[33] C. Gonzalez, H. B. Schlegel, *J. Phys. Chem.* **1990**, *94*, 5223.
[34] G. Landrum, *YAeHMOP*, Cornell University, Ithaca, New York, **1995**.
[35] A. F. Shestakov, A. E. Shilov, *Zh. Obshch. Khim.* **1995**, *65*, 60; b) *J. Mol. Catal. A: Chemical* **1996**, *105*, 1.
[36] W. E. Billups, S.-C. Chang, R. H. Hauge, J. L. Margrave, *J. Am. Chem. Soc.* **1993**, *115*, 2039; b) W. E. Billups, S.-C. Chang, R. H. Hauge, J. L. Margrave, *ibid.* **1995**, *117*, 1387.
[37] See for example, a) W. A. Goddard, *Science* **1985**, *227*, 917; b) H. F. Schaefer, *ibid.* **1986**, *231*, 1100.
[38] E. A. Carter, W. A. Goddard, *J. Phys. Chem.* **1988**, *92*, 2109.
[39] A. Fiedler, J. Hrušák, W. Koch, H. Schwarz, *Chem. Phys. Lett.* **1993**, *211*, 242.
[40] D. E. Clemmer, Y.-M. Chen, F. A. Khan, P. B. Armentrout, *J. Phys. Chem.* **1994**, *98*, 6522.